FRACTIONAL FLUXON DYNAMICS IN LONG JOSEPHSON JUNCTIONS

by

Lawrence Antonio Rhoads, B.S

THESIS

Presented to the Faculty of

The University of Houston-Clear Lake

In Partial Fulfillment

Of the Requirements

For the Degree

MASTER OF SCIENCE

in Physics

THE UNIVERSITY OF HOUSTON-CLEAR LAKE

DECEMBER, 2020

FRACTIONAL FLUXON DYNAMICS IN LONG JOSEPHSON JUNCTIONS

by

Lawrence Antonio Rhoads, B.S

APPROVED BY

_____
Van Eric Mayes, PhD, Chair

_____
David Garrison, PhD, Committee Member

_____
Samina Masood, PhD, Committee Member

APPROVED/RECEIVED BY THE COLLEGE OF SCIENCE AND ENGINEERING:

_____
Miguel Gonzalez, PhD, Dean

_____
David Garrison, PhD, Interim Associate Dean

DEDICATION

I dedicate this thesis to my family. They were with me throughout the entire process, and anything I do that makes the world a better place is due to their affect on my person.

ACKNOWLEDGMENTS

First and foremost, I am grateful to my advisor, Dr. Van Mayes, for being friendly, caring, supportive, and helpful in numerous ways. Without his support, I could not have finished this project. He was very generous in sharing his experiences on theoretical research, academic life and beyond. I would also like to acknowledge Dr. Ju H. Kim for his efforts in advising and educating me in the overall field, as well as providing me with the starting point for the necessary theoretical background. I am also grateful to Dr. David Garrison for his helpful advice on the numerical computations and on the stability section of this thesis. I acknowledge Dr. Samina Masood for her helpful edits and advice for the introductory chapter. I would also like to acknowledge Ram Shoham and Jordan Gemmill for their contributions in deriving the solutions to the equations of motion. I would also like to thank Jonathon Miller, for his edits to previous drafts of this work.

ABSTRACT

FRACTIONAL FLUXON DYNAMICS IN LONG JOSEPHSON JUNCTIONS

Lawrence Antonio Rhoads, B.S

University of Houston-Clear Lake, 2020

Thesis Chair: Van Eric Mayes, PhD

In this thesis, I investigate the dynamics of fractional fluxons in two-gap Long Josephson Junctions (LJJs). Due to time reversal symmetry (TRS) breaking within the LJJ, a single fluxon may split into a bound pair of fractional fluxons, behaving as a sort of quasi-molecule. While fractionated, the fluxon pair is bound together by an interaction potential, which is repulsive at short distances, but attractive at longer distances, relatively speaking. In order to induce TRS breaking, an external bias potential and a pinning potential is introduced, representing an external current and a micro-resistance, into the initial equation of motion, the Double Sine-Gordon Equation (DSG). Using a software called freefem++, I simulate a LJJ with experimental parameters that allow for broken TRS, and so has fractional fluxon dynamics. After confirming fractional fluxons were present, I calculate the tunneling rate through the potential barrier for each fluxon. The tunneling rate was found to be in agreement with previous results for a single fluxon for the large fluxon, and not for the smaller fluxon.

TABLE OF CONTENTS

LIST OF TABLES

LIST OF FIGURES

CHAPTER 1

OVERVIEW

Quantum computation is the study of computer systems that utilize the unique properties of quantum mechanics in order to carry out operations that can solve problems in much less time than in classical computer systems[37]. The quantum nature of the information carriers in a quantum computer allow for interesting applications that are otherwise not possible. For example, factoring a 2048-bit-long number would take a classical computer longer than the age of the universe, whereas a quantum computer running at 100MHz would factor the number in a few hours [38]. This is possible due to taking advantage of the superposition postulate of quantum mechanics.

In classical computation, every bit of information is in a definite state, usually defined as being in the 1 or 0 state. In quantum computation however, quantum bits (qubits) are usually in a state of superposition of "1" and "0". This allows calculations to be carried out in parallel using the "same" qubits, since they are not in any particular state. As a consequence, if you built a quantum computer with N qubits you would get a 2^N increase in computing power as opposed to the non-exponential behavior of classical computing. However, there are some challenges in using qubits that need to be addressed before we can take advantage of this increase in computing power. Since the qubit is in a state of superposition, any interaction with the surrounding environment may cause the system to collapse into either state which makes up the superposition, thus losing the superposition and any quantum behavior being utilized for computation. This phenomenon is known as decoherence[11][41][48], and it is one of the largest obstacles to building a quantum computer with many qubits. Decoherence also poses a problem when trying to connect quantum computational systems to classical systems. In order to read any information in the quantum com-

puter, there must eventually be an interface with a classical readout machine, which poses a danger to the stability of the quantum system doing the calculations.

In spite of these challenges the potential benefits of quantum computing outweigh the imposing obstacles we face. Currently there is a great deal of research in the physical systems that can be used to create and manipulate qubits. Qubits can be made out of many different systems and each system has its own benefits and detriments. A quantum computer must have three factors to be viable; scalability, correctability, and universal logic[37]. In order to achieve these characteristics, many different physical systems are being researched, designed, and tested in order to create viable quantum computers. Out of the many candidates for qubit systems there is the possibility of using superconducting systems. Superconducting quantum computing is an attractive alternative because such systems can be precisely fabricated using existing technology to have a range of desirable properties[39][47][10]. In superconducting systems, there are many different ways to create a qubit and the necessary logic gates required to manipulate them. There are charge qubits, such as the Cooper Pair box[6], flux qubits[17], and phase qubits[40]. Josephson junctions are one way to create these qubits and based on the designs and various properties of the device we can create one or all three kinds of qubit.

A Josephson junction is a device composed of two weakly interacting superconductors separated by thin insulating layer. Josephson junctions have been a subject of interest for a long time now, since the 1960s, and they still hold a central place in both quantum computing and condensed matter research in general. One of the most interesting things about Josephson junctions is that they are clear examples of have macroscopic behaviors that are driven by quantum mechanics. The phase difference of the magnetic flux inside a Josephson junction is a prime example[18] and is the foundational phenomenon for this thesis.

In this thesis, I will be examining the phase dynamics of a Long Josephson Junction (**LJJ**) made with two "two-gap" superconductors, with a micro-resistor added in and a bias current driven through it. This creates an ideal environment to exhibit an unusual behavior in the magnetic flux which travel within the insulating layer of the device. Under these conditions the flux quanta, called **fluxons** from now on, can be separated into two distinct but bound "fractional" fluxons long enough to observed. Using the **finite element method (FEM)**, I will demonstrate that the separation of these **fractional fluxons** can be stable long enough to be observed experimentally. I will show that with an appropriate choice of external parameters each fractional fluxon has a distinct energy minima when pinned to the micro-resistor, and has a small enough tunneling rate for experimental observation.

This thesis is divided into three parts. The first part explains the theoretical background this research is based on. I review the Josephson effect(s) the different equations of motion which describe Josephson junctions, then derive and examine the main equation we will be working with, the double Sine-Gordon equation. I will also briefly explain the mechanism behind the fractionalization of fluxons in multi-gap superconducting Josephson junctions. In the Methods and Results chapter, I examine the total potential associated with the inhomogenous (perturbed) double Sine-Gordon equation, broken into external and interaction potentials. Then I review the Finite Element Method as well the external and interaction potentials for fractional fluxons. Then the numerical results are examined and confirmed via observation of the magnetic profiles for the solutions. Finally, I calculate of the macroscopic tunneling rate for a fractional fluxon pair in a LJJ for a given set of experimental parameters in order to ensure the fractional fluxons can be observed in experiment. In the conclusion, I summarize the results of my research, discuss the implications and outline future directions that may be pursued.

CHAPTER 2

THEORETICAL BACKGROUND

2.1   Introduction

When talking about the dynamics of Josephson Junctions, it's important to discuss the theoretical underpinnings of the dynamics therein. The type of Josephson Junctions we are interested in are called **Long Josephson Junctions (LJJs)**. LJJs are Josephson Junctions where one or more sides of the device is much longer than the **Josephson penetration depth** λ_J[17].

Among the various materials used to make LJJs, those made from iron-based superconductors are of special interest[28]. These LJJs, under the right conditions, may exhibit time reversal symmetry breaking[27], which allows for the loops of magnetic flux (i.e fluxons) to separate into a bound pair of fractional fluxons.

LJJs are of interest for a variety of reasons ranging from SQUIDs, superconducting single-electron transistors[21], to RSFQ digital electronics. However, it is the applications to quantum computing are the motivation behind this thesis. Fluxons can be used as qubits and have several advantages to other qubit candidates. Fluxon qubits exhibit significantly longer decoherence times than other types of qubits[32] and are much easier to integrate with classical readout components.

2.2   Long Josephson Junctions

Long Josephson Junctions have been studied for a long time[43] and much progress has been made in understanding how they work. A Long Josephson Junction is a Josephson Junction where one dimension is significantly longer than the others. To be more specific, in order to call a Josephson Junction a "Long" Josephson Junction,
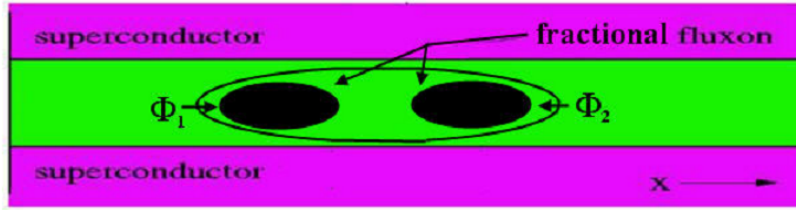
Figure 2.1: *Due to the broken time-reversal symmetry (BTRS) state, a single fluxon can split into a bound pair of fractional fluxons.*

at least one dimension needs to be much longer than the **Josephson penetration depth,** λ_J. LJJs are fabricated by placing an insulating material between two superconducting materials. The standard way to represent this is to refer to this design as a **Superconductor-Insulator-Superconductor (S-I-S)** LJJ. There are other ways to elicit the Josephson Effect, but I will not discuss them as the model in question uses the S-I-S design.

Long Josephson Junctions made with iron based superconductors[28] experience two Josephson effects, one from superconducting Cooper pairs tunneling within the same electronic band as well as the **Inter-band Josephson Effect** which is tunneling from one band to another. In some circumstances it is possible to have time reversal symmetry break, which causes the magnetic flux quanta (fluxons) which form to fracture into two coupled fluxons, which we call **fractional fluxons**. The properties of these fractional fluxons will be discussed in detail later.

2.2.1   Josephson Effect

In 1962 Brian Josephson predicted that under certain conditions a supercurrent can flow even without an applied voltage in a pair of superconductors weakly coupled together with an insulating barrier, provided the barrier was thin enough[29]. This

assembly is called a Josephson junction, and the current that flows between the superconducting layers is called the Josephson Effect[8].

Assume a device constructed by taking two superconductors, **A** and **B**, with a thin insulating barrier **C** separating them. We can define a "pseudo-wave function" which represents the wave functions of the Cooper pairs in each superconductor as $\Psi_L = \sqrt{n_L} \exp(-i\varphi^L)$ where L is either superconductor **A** or **B** and n_L is the density of the electrons moving in the L-th layer. Then we let the potential difference across the superconductor layers be written as $2eU$ where e is the charge of the electron. Then for the system we have a two-state Schrödinger equation[1],

$$i\hbar\frac{\partial}{\partial t}\begin{pmatrix} \sqrt{n_A}\exp(-i\varphi^A) \\ \sqrt{n_B}\exp(-i\varphi^B) \end{pmatrix} = \begin{pmatrix} eU & K \\ K & eU \end{pmatrix}\begin{pmatrix} \sqrt{n_A}\exp(-i\varphi^A) \\ \sqrt{n_B}\exp(-i\varphi^B) \end{pmatrix} \tag{2.1}$$

with K being some constant that will depend on the actual LJJ. Solving the equation gives the following solutions[9]:

$$\dot{n_A} = \frac{2K\sqrt{n_A n_B}}{\hbar}\sin\Delta\phi \tag{2.2}$$

$$\dot{n_B} = -\frac{2K\sqrt{n_A n_B}}{\hbar}\sin\Delta\phi \tag{2.3}$$

$$\dot{\varphi_A} = -\frac{1}{\hbar}(eU - K\sqrt{\frac{n_B}{n_A}}\cos\Delta\phi) \tag{2.4}$$

$$\dot{\varphi_B} = \frac{1}{\hbar}(eU - K\sqrt{\frac{n_A}{n_B}}\cos\Delta\phi) \tag{2.5}$$

where $\Delta\phi = \varphi_B - \varphi_A$. Note that n_L is the charge carrier current density, so the time derivative of n_L can be interpreted as the current flowing through the superconductor. Then the equations we use to describe the Josephson Effect are,

$$I_s = I_c \sin(\Delta\phi) \tag{2.6}$$

$$V = \frac{\hbar}{2e}\frac{\partial\Delta\phi}{\partial t} \tag{2.7}$$

where I_s is the superconducting current and I_c is the critical current, the maximum super-current the junction can handle, and V is the voltage. The term $\Delta\phi$ is the phase difference of the two superconductors. Using the above form is difficult to use because the phase difference doesn't have gauge invariance,which can be addressed by substituting,

$$\gamma \equiv \Delta\phi - (\frac{2\pi}{\Phi_0}) \int \overrightarrow{\mathbf{A}} \bullet d\mathbf{s}$$

with $\overrightarrow{\mathbf{A}}$ being the vector potential, not to be confused with superconductor $\mathbf{A}$. Then the ideal Josephson junction is described by the following equation,

$$I_s = I_c \sin(\gamma) \tag{2.8}$$

The term γ is used to address the issue of the lack of gauge invariance in the phase difference between $\mathbf{A}$ and $\mathbf{B}$. If there is no magnetic field present then γ and $\Delta\phi$ are equivalent. For the remainder of the thesis we will be signifying the phase difference between the two superconductors by $\Delta\phi = \phi$ and most of my results assume there is no external magnetic field being applied.

2.2.2 Inter-band Josephson Effect

The previous section dealt with the classic Josephson Effect, where current runs between two superconductors. There is another type of Josephson Effect that can exist in certain types of superconductors. In multi-gap superconductors such as iron-pnictides[35], there can be a phase difference that exists between different electron condensates (or bands) within the same superconductor. This is called the **inter-band Josephson Effect**, and for some Josephson junctions, it can complicate the phase dynamics in the system.

This inter-band phase difference, which we will denote as χ arises from the tunneling of Cooper pairs from one electronic band to another within the same layer.

Because multi-gap superconductors have more than a single tunneling channel, they are described with multiple "pseudo-order parameters", which will be further explained in the coming sections. In this thesis, I will specifically deal with two-gap superconductors, which have two tunneling channels for Cooper Pairs, for the s-band and the d-band condensates.

2.3   Phase Dynamics

The phase dynamics within a LJJ can be modeled using Ginzburg-Landau theory for superconductors. This model describes the behavior using a complex psuedo-order parameter, $\Psi_\ell = \psi_\ell \exp(-i\theta^i)$ which describes the phase in the ℓ-th layer. ψ_ℓ is the amplitude and θ^i is the phase angle in the i-th electronic band. The inter-band pairing of electrons depends on the relative phase difference between different bands in the same superconductor layer, $\chi_\ell = \theta_\ell^s - \theta_\ell^d$. The description of the energy of a two-gap LJJ can be written as a Hamiltonian,

$$\mathcal{H} = f_\ell^s(|\psi_\ell^s|^2) + f_\ell^d(|\psi_\ell^d|^2) - V_{ss}|\psi_\ell^s|^2 - V_{dd}|\psi_\ell^d|^2 - V_{sd}(\psi_\ell^{*s}\psi_\ell^d + \psi_\ell^{*d}\psi_\ell^s) \qquad (2.9)$$

Where f_ℓ is the free energy for the s or d band in the ℓ-th layer, and V is the potential between electrons in the same band or in different bands. $f_\ell^s(|\psi_\ell^i|^2)$ is the kinetic energy of electrons in the i-th band. If there is no disruption of the time reversal symmetry of the system then the last term would go to zero or when there is no inter-band contribution at all.

2.3.1 Time Reversal Symmetry

When a LJJ is created with $J < 0$, the system exhibits **time-reversal symmetry** (**TRS**), which is the property that when

$$t \rightarrow -t$$

then,

$$\Psi_\ell \rightarrow \Psi_\ell^*$$

and nothing changes with respect to the system.

However, in two-gap LJJs there are instances when this symmetry is broken. We call this the **Broken Time-Reversal Symmetry** (**BTRS**) state[45][22]. When a LJJ is in the BTRS state,

$$\Psi_\ell \neq \Psi_\ell^*$$

which leads to the inter-band energy contribution in $\mathcal{H}$, not being canceled out in the Hamiltonian, $\psi_\ell^{*s}\psi_\ell^d + \psi_\ell^{*d}\psi_\ell^s \neq 0$, which leads to the need to use a different equation of motion for the phase dynamics.

2.3.2 Single Fluxon

A single fluxon is modeled by the sine-Gordon equation (**SGE**)[4],

$$\phi_{tt} - \phi_{xx} + \sin(\phi) = 0 \tag{2.10}$$

and has two solutions, one for "breathers" and one for "kinks". The solution we are interested in is the kink solution,

$$\phi(x,t) = 4\arctan(\exp(\gamma(x-\nu t))) \tag{2.11}$$

where γ is,

$$\gamma = \sqrt{\frac{1}{1-\nu^2}}. \tag{2.12}$$

Note that these equations and solutions are normalized[24] using the Josephson penetration depth λ_J and the Josephson plasma frequency ω_p, and ν is the velocity of the fluxon normalized to the Swihart velocity $\bar{c} = \lambda_J\omega_p$. There many ways to solve the SGE to get this solution, and when a two-gap LJJ is in the TRS state, this is the correct way to model the fluxon behavior.

However when time-reversal symmetry is broken, there are additional effects due to the inter-band Josephson effect previously discussed and it becomes necessary to use the Double sine-Gordon Equation (**DSG**) to model the fluxon behavior.

2.3.3   Fractional Fluxons

In the case of multi-gap LJJs, we must use the double Sine-Gordon equation[20][13][25],

$$\phi_{xx} - \phi_{tt} + \sin\phi + \frac{J}{2}\sin 2\phi = 0 \tag{2.13}$$

The coefficient J is given by the parameters of the LJJ. When $J \leq 1$ the Sine-Gordon equation describes the system, but when $J > 1$ we must use the double Sine-Gordon equation. The kink solution for this equation can take two forms, one for the larger fluxon and one for the smaller fluxon. The next section will solve the DSG equation and after we will find some qualitative information about how the fluxons fractionate.

The two solutions are complementary, meaning that they add together to the single fluxon solution. This is why they are treated as "fractional" fluxons rather

than distinct fluxons. This is also a good way to check the integrity of our solutions, since if they don't add together into a single fluxon, they can't be considered true fractional fluxons.

2.3.3.1 Solutions to the Double Sine-Gordon Equation

The DSG equation can be rewritten into

$$\phi_{xx} - \phi_{tt} - \sin\phi[1 - J\cos\phi] = 0.$$

We then make the following assumptions concerning ϕ. First, let ϕ be a function such that $\phi(x,t) : x \in \mathbb{R}, t > 0$. Second, let ϕ be a smooth, continuous function with the derivative at $x = \pm\infty$ be zero. Now we make a substitution so that ϕ is a function of the collective coordinate $(\zeta = x - \nu t)$. Making the change of variables,

$$\left(1 - \nu^2\right)\frac{\partial^2\phi}{\partial\zeta^2} = \sin\phi[1 - J\cos\phi].$$

We then make use of the power rule for derivatives on the LHS,

$$\left(1 - \nu^2\right)\frac{1}{2}d\left(\frac{d\phi}{d\zeta}\right)^2 = \sin\phi[1 - J\cos\phi]d\phi.$$

Letting $(u = 1 - J\cos\phi)$ we integrate the RHS, and after a bit of algebra we are left with

$$\frac{d\phi}{d\zeta} = \frac{\pm 1}{\sqrt{J(1 - \nu^2)}}(1 - J\cos\phi). \tag{2.14}$$

The "$\pm$" lets us choose whether we will be solving for kinks or anti-kinks, so the choice is a little arbitrary, as we can always adjust our coordinates to fix it if we need to.

Regardless, this sets us up for the integral

$$\int \frac{d\phi}{1 - J\cos\phi} = \int \frac{\pm d\zeta}{\sqrt{J(1 - \nu^2)}}$$

The integral on the LHS is evaluated from some arbitrary initial point ζ_0 to ζ,

$$\int_{\zeta_0}^{\zeta} \frac{d\phi}{1 - J\cos\phi} = \Bigg|_{\zeta_0}^{\zeta} - \frac{2\left(\tanh^{-1}\left(\sqrt{\frac{J+1}{J-1}}\tan\left(\frac{\phi(\zeta)}{2}\right)\right) - \tanh^{-1}\left(\sqrt{\frac{J+1}{J-1}}\tan\left(\frac{\phi(\zeta_0)}{2}\right)\right)\right)}{\sqrt{J^2 - 1}}$$

which makes the LHS and RHS,

$$-\frac{2\left(\tanh^{-1}\left(\sqrt{\frac{J+1}{J-1}}\tan\left(\frac{\phi(\zeta)}{2}\right)\right) - \tanh^{-1}\left(\sqrt{\frac{J+1}{J-1}}\tan\left(\frac{\phi(\zeta_0)}{2}\right)\right)\right)}{\sqrt{J^2 - 1}} = \frac{\pm(\zeta - \zeta_0)}{\sqrt{J(1 - \nu^2)}}.$$

Taking the negative solution, letting $(\zeta_0 = 0)$, and solving for $\left(\tan\left(\frac{\phi(\zeta)}{2}\right)\right)$

$$\tan\left(\frac{\phi(\zeta)}{2}\right) = \frac{\tanh\left(\zeta\sqrt{\frac{J^2-1}{4J(1-v^2)}} + \tanh^{-1}\left(\sqrt{\frac{J+1}{J-1}}\tan\left(\frac{(\phi(0))}{2}\right)\right)\right)}{\sqrt{\frac{J+1}{J-1}}} \tag{2.15}$$

From here $\phi(0)$ may take on two values, either 0 or π. This is due to the boundary conditions we set earlier. Letting $\phi(\zeta = 0) = 0$ and solving eq. 2.15 for $\phi(\zeta)$ results in

$$\phi(\zeta) = 2\tan^{-1}\left(\sqrt{\frac{J-1}{J+1}}\tanh\left(\sqrt{\frac{J^2-1}{4J(1-v^2)}}\zeta\right)\right) \tag{2.16}$$

If we take $\phi(\zeta = 0) = \pi$ we then get,

$$\phi(\zeta) = 2\tan^{-1}\left(\sqrt{\frac{J-1}{J+1}}\coth\left(\sqrt{\frac{J^2-1}{4J(1-v^2)}}\zeta\right)\right) \tag{2.17}$$

These two solutions represent the fractional fluxons in the system. Substituting some of the values to make it cleaner we can represent these solutions as,

$$\phi^> = 2\tan^{-1}(a\tanh(bq)) \qquad\qquad a = \sqrt{\frac{J-1}{J+1}} \tag{2.18}$$

$$\phi^< = 2\tan^{-1}(a\coth(bq)) \qquad\qquad b = \sqrt{\frac{J^2-1}{4J}} \tag{2.19}$$

$$q = \frac{\zeta}{\sqrt{1 - v^2}}$$

12

Where eq. 2.18 is the larger fluxon and eq. 2.19 is the smaller fluxon. As for the constants a and b, they clearly scale the kink as J grows. It is notable that as J
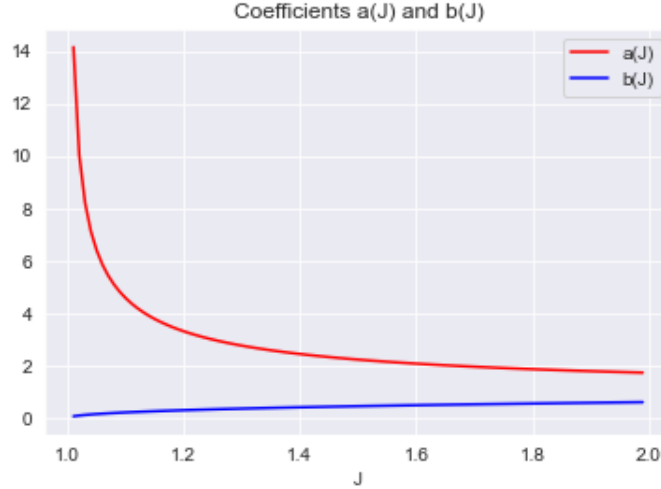
Figure 2.2: *It is clear that as J becomes increasingly greater than 1, a and b approach each other.*

increases, they quickly approach each other. Figure 2.2 shows another interesting quality for these constants, and that is that $a \to \infty$ as J gets closer to 1. This shows why the regime for the DSG is for values of $J > 1$.

2.3.4 Fractional Behavior

Consider the DSG equation in the previous subsections. Looking at the behavior of the equation of motion we can tease out some qualitative behavior that can be used to motivate our numerical study[7]. For example, if we take a look at the terms $\sin \phi + (J/2) \sin 2\phi$ we can get a feel for how the fluxon(s) should behave when the

boundary condition $\phi'(x = \pm\infty) = 0$ is applied.

$$\sin\phi + \frac{J}{2}\sin 2\phi = 0$$

$$\sin\phi(1 + J\cos\phi) = 0$$

This implies that either $\phi = 0$ or $\phi = n\pi$, which we made use of in solving the DSG, and also,

$$1 + J\cos\phi = 0$$

$$\phi_J \rightarrow \phi = \cos^{-1}(\frac{1}{J}) \tag{2.20}$$

Which gives us a way to bound the fractional behavior of the system.

In the case of $J > 1$ the fractional fluxons will distribute over space such that the first fluxon will increase like $\phi(x = -\infty) = -\phi_J$ to $\phi(x = +\infty) = \phi_J$. The second fluxon will then go from $\phi(x = -\infty) = \phi_J$ to $\phi(x = +\infty) = 2\pi - \phi_J$. Note that the phase difference $\phi(x = +\infty) - \phi(x = -\infty)$ has for the two fluxons,

$$\phi_< = \frac{\phi_J}{\pi}\Phi_0, \qquad\qquad \phi_1 < \frac{\Phi_0}{2} \tag{2.21}$$

$$\phi_> = (1 - \frac{\phi_J}{\pi})\Phi_0, \qquad\qquad \phi_2 > \frac{\Phi_0}{2} \tag{2.22}$$

where Φ_0 is the single fluxon value. Clearly we can label $\phi_<$ to be the small fluxon and $\phi_>$ the large fluxon.

2.4   Nonhomogeneous Double Sine-Gordon Equation

When considering a LJJ with a micro-resistance implanted into some part of the device and running a bias current through the device, we must add a term to the

DSG[42] and treat it a a perturbation[44],

$$\phi_{xx} - \phi_{tt} + \sin\phi + \frac{J}{2}\,\sin2\phi \; = F. \tag{2.23}$$

Considering a dissipation-less system, F contains a term for the bias current and the micro-resistance[36],

$$F = \epsilon\sin(\phi)\delta(x - x^i) - f_b, \tag{2.24}$$

where $\delta(x - x^i)$ is the delta Dirac distribution, f_b is the bias current and $\epsilon > 0$ is the normalized strength of the micro-resistance[30]. ϵ is defined as,

$$\epsilon = \frac{(j_c - j_c')b}{j_c\lambda_J} \tag{2.25}$$

where λ_J is the Josephson penetration depth, and j_c, j_c' is the critical current density and reduced critical current density near the micro-resistance respectively. Experimentally the value of the sheet resistance from such a set up has been found to be around 1Ω[3]. In order to justify the use of the delta Dirac distribution to model the micro-resistance, we need $b << \lambda_J$, which will set the limit $\epsilon << 1$. For the rest of this work, for convenience we will set $J/2 = J$ since it is a constant.

CHAPTER 3

METHODS AND RESULTS

3.1 Introduction

This chapter discusses the numerical simulations I performed on a fractional fluxon pair pinned in a LJJ by a single micro-resistance at some point in the LJJ. The external potential is comprised of the bias current and the pinning potentials. We neglect the dissapative terms[6] as well as the critical current fluctuation.The external potential, $U_{ext} = U_{bias} + U_{pin}$, can be calculated for both the single fluxon as well as the fractional fluxon pair. For the fractional fluxon, there is also an interaction potential, $U_{int} = U_{attr} + U_{rep}$, which will be investigated but, as we will see, seems to have a small effect on the behavior of the fractional fluxon, and for our purposes may be neglected without changing the system's behavior.

First, we will calculate the local minimum for the fractional fluxon pair, then we will use those values to solve the Double Sine Gordon equation for the fluxon pair using the finite element method (FEM). We will then plot the magnetic profiles to see if the separation can be observed, then the macroscopic quantum tunneling rate Γ will be calculated to ensure that the pair will be pinned to the micro-resistance long enough to be observed. It will also be shown that the interaction potential doesn't affect the simulation for the fluxon pair that much and can be neglected without losing the fractional behavior of the fluxon in the LJJ.

3.2 Local Minima

We can find the local minimum of the total potential for a fractional fluxon pair by fixing the bias current, pinning resistance, and the inter-band Josephson coefficient,
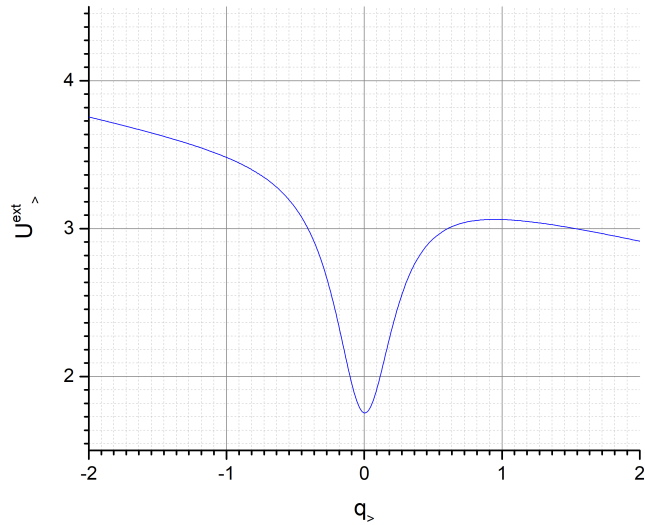
Figure 3.1: *A plot of the external potential of the greater fluxon with J= 1.15, f=0.03, and epsilon = 0.85.*

then using a minimization algorithm to find q_1 and q_2. Using a simple script found in the appendix, we found the minima for each fluxon to be at a different point in the LJJ, as we will see in a moment. First, I shall define the potential functions used in the minimization.

3.2.1 External Potential

The external potential is the potential due to the bias current and the micro-resistance, respectively called the **bias potential** and the **pinning potential**, and is found analytically using methods from references [12] and [15] to be
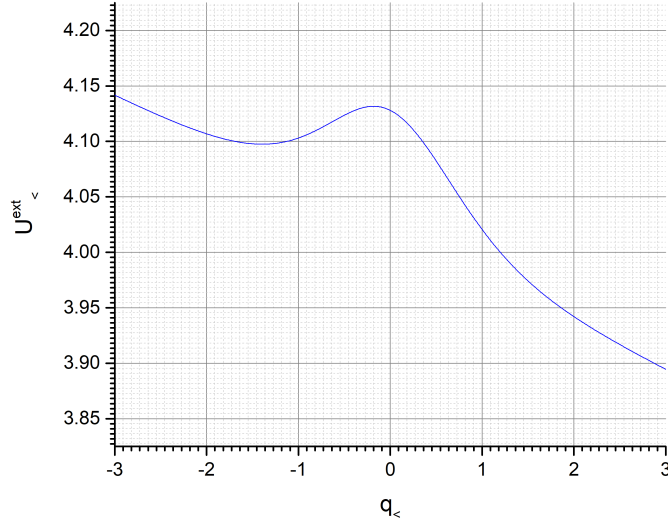
Figure 3.2: *A plot of the external potential of the lesser fluxon with J= 1.15, f=0.03, and epsilon = 0.85.*

$$U_{ext} = U_{bias} + U_{pinning} \qquad \text{Total external potential}$$

$$U_{bias} = -\sum_{i=1}^{2} \int f_i \phi_i dx \qquad \text{Bias potential}$$

$$U_{pin} = \sum_{i=1}^{2} \int \epsilon_i \delta_i (x - x_i^0)(1 - \cos \phi_i) dx \qquad \text{Pinning potential}$$

where ϕ_1 and ϕ_2 are the large and small fluxon respectively. For the single fluxon, we use the solution for the Sine-Gordon equation. Substituting $\phi(x,t)$ into the potential functions we get,

$$U_{ext} = -2\pi f q - \frac{2\epsilon}{\cosh^2(q)}. \tag{3.1}$$

This potential has a meta-stable point, which the fluxon may arrive at if f and ϵ are chosen correctly. In order to see if there is a similar meta-stable point for the case when there are fractional fluxons, we need to use the solutions for each fluxon

J	f	ϵ	$q_{min} = (q_1, q_2)$
1.15	0.03	0.85	$(0.005, -1.565)$
1.15	0.01	0.85	$(0.005, -2.175)$
1.15	0.005	0.85	$(0.005, -2.525)$
1.10	0.03	0.85	$(0.005, -1.475)$
1.10	0.01	0.85	$(0.005, -2.085)$
1.10	0.005	0.85	$(0.005, -2.445)$
1.05	0.03	0.85	$(0.005, -1.275)$
1.05	0.01	0.85	$(0.005, -1.925)$

Table 3.1: *Local minima for the external potentials for each fractional fluxon.*

and see if there is a minima for both or neither solution. Substituting the solutions for the Double Sine-Gordon Equation into the above equations, we find the external potential U_{ext} for ϕ_1 and ϕ_2 to be,

$$U_{bias}^1 = -4\tanh(a)f_1 q_1 \tag{3.2}$$

$$U_{pinning}^1 = 2\epsilon_1[1 - \frac{1}{1 - a^2\tanh^2(q_1)}] \tag{3.3}$$

$$U_{bias}^2 = -[2\pi - 4\tanh(a)]f_2 q_2 \tag{3.4}$$

$$U_{pinning}^2 = 2\epsilon_1[1 - \frac{1}{1 - a^2\coth^2(q_2)}] \tag{3.5}$$

Thus,

$$U_{ext} = U_{ext}^1(q_1) + U_{ext}^2(q_2) \tag{3.6}$$

Where each $q_i = \dfrac{x_i - \nu t}{\sqrt{1 - \nu^2}}$.

Note, each external potential is only dependent on one fluxon. Notice in Table 3.1 that the minima for the large fluxon is fairly stable compared to the smaller fluxon. This may be a result of the relative size of the fluxons, such that the smaller fluxon may be more sensitive to the external parameters than the larger fluxon. At this point we have not yet included the interaction potential between the two fractional fluxons.

3.2.2 Interaction Potential

Unlike the case with a single fluxon, there is an interaction potential between the fractional fluxon pair that needs to be considered, and comes in two parts. There is an **attractive potential**, and a **repulsive potential**,

$$U_{int} = U_{attr} + U_{rep} \qquad \text{Total interaction potential}$$

$$U_{attr} = C_1 \frac{a^2 m_{sol}^1}{2b^2(1+a^2)} \ln(\cosh^2(bq) + a^2 sinh^2(bq)) \qquad \text{Attractive potential}$$

$$U_{rep} = 4C_2 a^2 b \int_{-\infty}^{\infty} AB dx' \qquad \text{Repulsive potential}$$

where C_1 and C_2 are constants and,

$$A = \frac{1}{\cosh^2(x') + a^2 \sinh^2(x')}$$

$$B = \frac{2}{-(1+a^2) + \frac{1}{2}(-1+a^2)K}$$

with

$$K = \cosh(2x')\cosh(2bq) - \sinh(2x')\sinh(2bq)$$

and

$$q = q_1 - q_2.$$

The repulsive part of the interaction potential is not easy to integrate, and so instead of solving it analytically it was numerically integrated and then a fitted function was found that approximated the solutions with an appropriate choice of coefficients, found in Table 3.2,

$$U_{rep} \approx \frac{k_1}{2} \left[\exp(-k_2(bq)^2) \frac{1}{\cosh(k_3 bq)} \right]. \tag{3.7}$$

J	k_1	k_2	k_3
1.05	0.252264	0.85	1.27
1.10	0.456957	0.82	1.23
1.15	0.634137	0.75	1.23

Table 3.2: *Numerical constants for the fitted function used for the repulsive potential.*

Bias Current	f	0.03
Micro-Resistance	ϵ	0.85
Josephson Coefficient	J	1.15

Table 3.3: *Experimental Parameters for the FEM Computations*

3.3   Numerical Analysis

I used FEM to solve the Double sine-Gordon equation using a fixed set of parameters. Previous work has discussed the validity of this method for the sine-Gordon equation[5], but I will show the stability in coming sections for completion. The table below describes the values for each parameter I fixed for each run. I used an open source software called freeFEM++[26] to run the program, and based my script on a one written by Caputo et.al[14] for Y-junctions. I found that the interaction potential doesn't play a significant part in the overall behavior of the system. Whether the interaction terms are included or not doesn't seem to affect the fracturing in any noticeable way.

Consider a scalar product of two functions in $\mathbf{L}_2(\Omega)$ space

$$(\phi, \psi) \equiv \int_\Omega \phi\psi \; dxdy.$$

The function ϕ is the same one in the Double Sine-Gordon equation, while ψ is called the "test function"[46] and only needs to be able to complete the inner product

space along with ϕ. Then, we use the scalar product to integrate the Double Sine-Gordon equation using Green's Theorem to find the "weak" form of the equation.

Using a two step discretization, we approximate the second derivative with respect to time as

$$\frac{\partial^2 \phi}{dt^2} \Rightarrow \frac{1}{(\Delta t)^2}\left(\phi^{n+1} - 2\phi^n + \phi^{n-1}\right) \tag{3.8}$$

where $n \in \mathbb{N}$ is the n-th time step and Δt is the time step size. The average of the Laplacian can be written by adding ϕ_n and $\phi n + 1$ and dividing by $\frac{1}{2}$,

$$\langle \nabla \phi \rangle = \frac{1}{2}\left(\phi^{n+1} + \phi^n\right). \tag{3.9}$$

Note, The choice to use ϕ_n and $\phi n + 1$ is so that at the initial time there will be a non-zero term for the Laplacian (section 3.2 of ref[46]). Combining all the terms and multiplying the DSG by ψ gives the final weak form for the perturbed Double Sine-Gordon Equation

$$\frac{1}{(\Delta t)^2}(\phi^{n+1} - 2\phi^n + \phi^{n-1}, \psi)$$
$$-\frac{1}{2}(\phi^{n+1} + \phi^n, \psi) + (\sin(\phi^n), \psi) + \frac{J}{2}(\sin(2\phi^n), \psi) \tag{3.10}$$
$$+(f + \epsilon\delta(x)\sin(\phi^n), \psi) = 0.$$

A short note on the Dirac distribution $\delta(x)$ in the perturbation. Since this distribution cannot be inputted into a numerical analysis, I used an approximate form which in the limiting case (as $\alpha \to 0$) approaches the same behavior as $\delta(x)$,

$$\delta(x) = \lim_{\alpha \to 0} \frac{1}{\alpha^2 \sqrt{\pi}} \exp(-\frac{x^2}{\alpha^2}). \tag{3.11}$$

After some trial and error, I used the value $\alpha = 0.005$ for my simulations as it was small enough to perform as a Dirac delta distribution while keeping my run time short enough to be productive.. This equation needs to be tested for stability, and we will do that using the conservation property of hyperbolic PDEs.

3.3.1 Stability

By keeping the time step Δt small the numerical simulation can be kept stable, and the stability can be checked by computing the energy of the system over the total simulation time. The time discretization method is stable according to the Von Neumann analysis and the weak form of the energy is conserved up to order $\mathcal{O}(h^4)$ [14] where h is the size step of the mesh, which in my case is $h = 1.0002$.

The energy of the system can be written in two parts,

$$d\varepsilon = E_{homo} + E_{pert} \tag{3.12}$$

where the two terms are the energy for homogeneous part of the equation and the energy for the perturbation. Plugging in the forms for each term of the energy we get,

$$\int d\varepsilon = \int d(\frac{1}{2}(\phi_t^2 + \phi_x^2) + (1 - \cos\phi) + \frac{1}{2}(1 - \cos(2\phi)) $$
$$+ f\phi + \epsilon\delta(x - x_0)(1 - \cos\phi)). \tag{3.13}$$

For the numerical simulation, the energy is discretized using,

$$\frac{d\phi}{dt} \Rightarrow \frac{\phi^{n+1} - \phi^{n-1}}{2\Delta t}$$

so the equation becomes

$$\int d\varepsilon = \int \frac{1}{2}d\left(\left(\frac{\phi^{n+1} - \phi^{n-1}}{2\Delta t}\right)^2 + (\nabla\phi^n)^2\right.$$
$$+ 2(1 - \cos\phi^n) + (1 - \cos(2\phi^n)) \tag{3.14}$$
$$\left. + 2f\phi + 2\epsilon\delta(x - x_0)(1 - \cos\phi))\right).$$

The plots of the total energy and the relative energy error show that the simulation
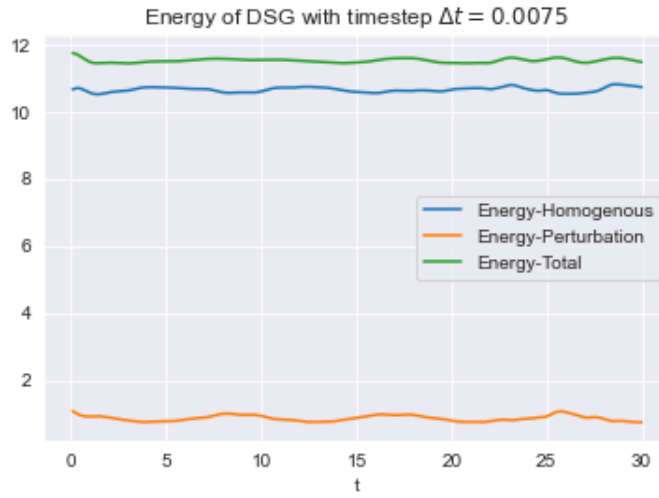
Figure 3.3: *The energy plotted with $\Delta t = 0.0075$ shows that the simulation is stable with the mesh element size at $h = 1.002$.*
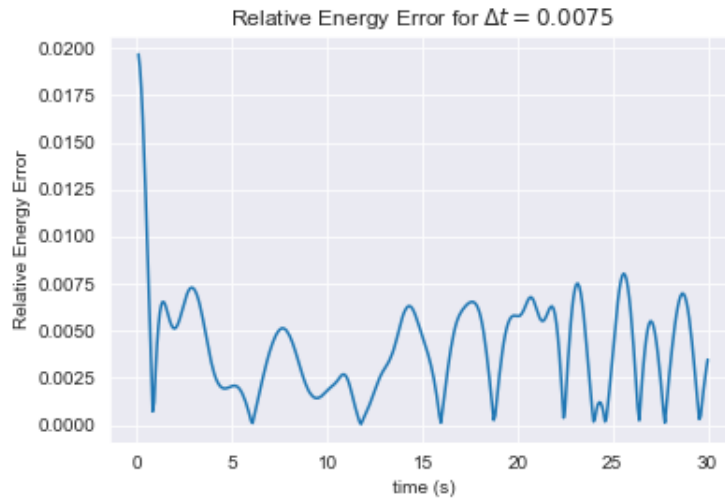
Figure 3.4: *A plot of the relative energy error $\dfrac{|E_n - <E>|}{<E>}$ where E_n is the energy at the n-th timestep and $<E>$ is the average of the computed energies in the system over the simulation time.*

conserves energy over the simulation time and so is stable. This means that we can have confidence in our system's results concerning the behavior of the fluxon in our LJJ.

3.4   Numerical Solutions
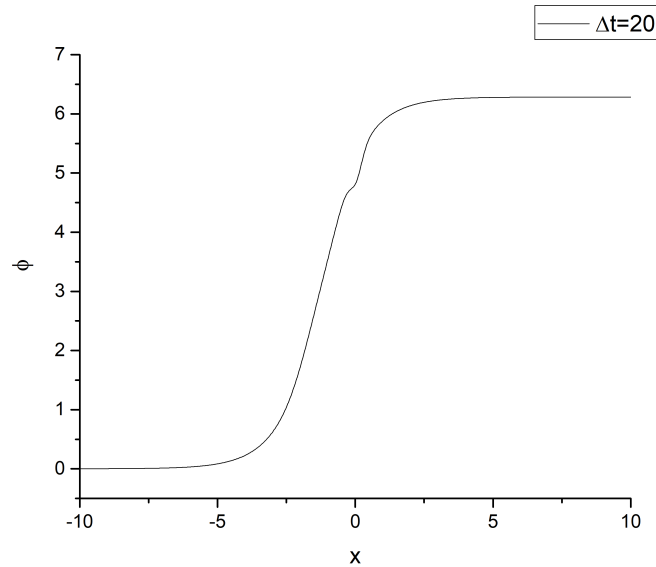
Figure 3.5: *Plotting ϕ vs x shows that the single fluxon splits into a large and small fluxon with $J > 1$.*

After running several numerical simulations using different values for parameters J, f, and ϵ, I did find fractional behavior in the LJJ. I have added the FEM script to the Appendix, as well as the script for the calculation of the external potential minima. By plotting ϕ over the x-direction it's noticeable at several times Δt that the single kink has become a double kink, as shown in Figure 3.5. It was not necessary to include the y-direction because the direction of travel for the kink solution we initialized for the DSG equation was made to be one dimensional. The micro-resistance was 2-D, because we found that the kink would warp around the micro-resistance if we made

25

it 1-D, which spoiled our simulations. However, it should be noted that many of the runs were quite noisy, so in order to be completely certain that what I was getting was in fact a true separation into two fractional fluxons, we needed to confirm their existence with an additional method of analysis.

3.5   Magnetic Profiles

One way to observe whether or not a fluxon did in fact split into a fractional fluxon pair is to view the magnetic profiles of the resulting flux and see if it is bimodal in shape. The magnetic profile is found by taking the derivative of our numerically calculated ϕ and plotting it over the mesh in one dimension. It is clear that after some time has elapsed in the simulation, the initial fluxon splits into two unequal fluxons.

Plotting the magnetic profiles for our simulations at different t, we see that there is a point in the simulation where the fluxon splits into a fractional fluxon pair. At the start of the simulation, $\Delta t = 0$ (Fig 3.6), the magnetic profile shows only a single mode which is indicative of a single fluxon, but at time $\Delta t = 20$ (see Fig 3.7) you can see there is a bimodal shape in the profile. This shows not only that there is fractionalization, but that the separation is large enough to be measured.

There is a bit of instability on the coherence of the bound pair, most likely because the fluxon pair is bound by a meta-stable potential, and so is naturally unstable. With some tuning, it could be that there are optimal parameters for achieving longer fractioning times. The question then remains whether the separation is maintained long enough to be measured before the pair tunnel through the barrier provided by the micro-resistance. This can be answered by calculating the macroscopic quantum tunneling rate for each fluxon, which I will do in the next section.
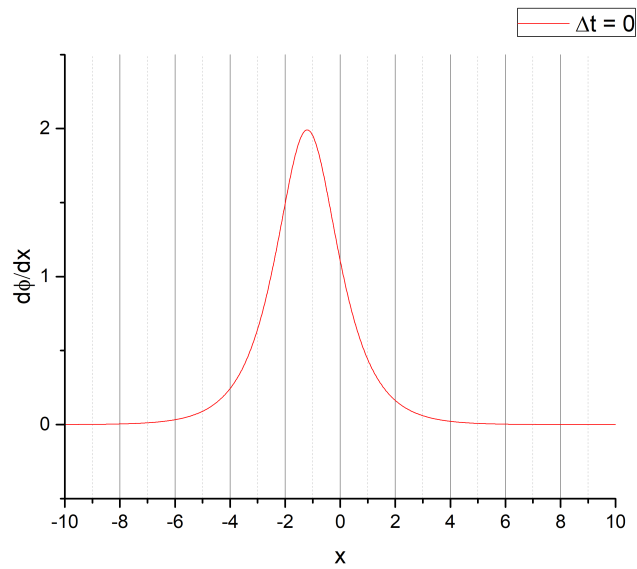
Figure 3.6: *The initial magnetic profile show an unfractionated fluxon.*
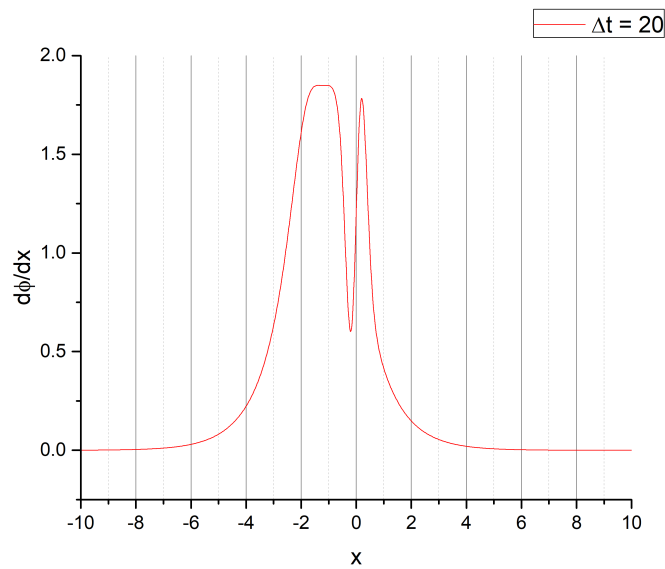
Figure 3.7: *The magnetic profile at t=20 shows two distinct peaks which is indicative of fractional fluxons.*

3.6   Macroscopic Quantum Tunneling

To calculate the quantum decay rate for a pair of fractional fluxons pinned in a two gap LJJ, we follow the method described in Kato et.al[30] for calculating the tunneling rate for a single pinned fluxon. Assuming the interaction between each fluxon pair is weak, we can calculate the tunneling rate Γ for each fluxon separately. The tunneling rate takes the form,

$$\Gamma = A \exp^{-B} \tag{3.15}$$

where B is the (non-trivial) path that minimizes the action of the fluxon. We found this when we found the minima for the external total potential. A is found as a function of the principle oscillation frequency at the meta-stable state ω_0, the Josephson plasma frequency ω_p, and B. A and B can only be determined in the limited case where the dampening coefficient, $\alpha + \dfrac{\beta}{3}$ is small enough to be ignored. This is the case for most actual experiments, so we can obtain the following expression,

$$A = \sqrt{60}\omega_0\omega_p\left(\frac{B}{2\pi}\right)^{\frac{1}{2}} \tag{3.16}$$

$$B = q_i \tag{3.17}$$

where q_i is either the small or large fluxon minima.

Using the set parameters in Table 3.4 and the values for everything else from Kato et.al[30], I calculated Γ for both fluxon while varying f and J. The average tunneling rates for the fluxons were

$$< \Gamma_{q_1} > \approx 2.11 X 10^4 \frac{1}{s} \tag{3.18}$$

$$< \Gamma_{q_2} > \approx 4.37 X 10^6 \frac{1}{s} \tag{3.19}$$

where q_1 and q_2 are the large and small fluxon respectively. The tunneling rate for the large fluxon are on the same order of magnitude with the tunneling rate calculated

J	f	ϵ	Γ_1	Γ_2
1.15	0.03	0.85	7.26×10^4	6.18×10^6
1.15	0.01	0.85	7.46×10^4	1.38×10^7
1.15	0.005	0.85	7.51×10^4	2.12×10^7
1.10	0.03	0.85	7.26×10^4	5.48×10^6
1.10	0.01	0.85	7.46×10^4	1.23×10^7
1.10	0.005	0.85	7.51×10^4	1.92×10^7
1.05	0.03	0.85	7.26×10^4	4.17×10^6
1.05	0.01	0.85	7.46×10^4	1.01×10^7

Table 3.4: *Tunneling rates for large (ϕ_1) and small (ϕ_2) fluxons.*

for the single fluxon case, $\Gamma \approx 2X10^4[\frac{1}{s}]$. The smaller fluxon had a much faster decay rate, which is expected as the effective mass of the fluxon is less, and so the energy required to tunnel passed the micro-resistance should also be less. These tunneling rates are large enough to observe in a laboratory, which gives me confidence that the pinned fractional fluxon pair is able to be experimentally verified.

Another way to examine the tunneling rates is to use equation 2.20 and equations 2.21 & 2.22 to find the approximate size of each fluxon as a fraction of Φ_0. For $J = 1.15$, we expect $\phi^< \approx 0.1644\Phi_0$ and $\phi^> \approx 0.8356\Phi_0$. This gives good support for the disparate tunneling rates as the two fluxons are very different in size and why the large fluxon's Γ is so similar to the single fluxon's value found in reference [30].

CHAPTER 4

CONCLUSIONS AND FUTURE WORK

4.1 Future Work

From the results of this research and the more recent findings in both multi-gap superconductors and quantum computing, there are several interesting directions for this research to go. The most obvious direction is to construct a flux qubit out of a two-gap LJJ, using a pair of micro-resistors to create a double well potential, and from that make a two state system. Then examine the stability of the flux-pair qubit in a noisy and dissipative environment, similar to the work done by Kim et. al for a single fluxon qubit[34][6]. The type of material used to make the two-gap LJJ will need to be investigated as well, so an investigation of fractional fluxons in different two-gap materials will also need to be done. Additionally, the two-state qubit can be tested to see how susceptible it is to decoherence by external interference[21], like when coupled to a resonant cavity[32] or perhaps as a part of a multi-junction system[31][33].

It will also be necessary to determine the stability of the fractional state when acting as information carriers in an array of coupled LJJs, which could be modeled after the work done in reference [33]. Another interesting area of research that could be promising is the affect multi-gap superconductors have when they are used to make topological superconductors[16][19]. If there is BTRS state within a topological multi-gap LJJ, how would the fractional fluxon pair behave? When introducing an inhomogeneity like a micro-resistance[2] into a topological superconductor, you change the topological order of the superconductor[23], which will affect the junction's behavior as a topological superconductor. There is some work that has been done investigating this phenomenon[49], but the results of this project could be used

to further investigate the phase dynamics of topological superconductors where inhomogeneities complicate the picture.

4.2   Summary

In this thesis, I have demonstrated that in Long Josephson Junctions made using two-gap superconductors there are circumstances where the fluxon within will fractionate into a bound pair of fractional fluxons which are complementary to each other. I have also shown that by inputting appropriate experimental parameters such as J, bias current f, and micro-resistivity ϵ, it is possible to induce this phenomenon. The main mechanism behind the fractioning is the inter-band Josephson effect not canceling out due to the system being in a state of broken time reversal symmetry. This asymmetry causes the single fluxon to separate into two complementary smaller, but not necessarily equal, fractional fluxons. I validated this by numerically solving the semi-classical equation of motion for a LJJ, the double Sine-Gordon equation, with J values greater than 1 and various values for f and ϵ using the finite element method. I approximated the Dirac delta distribution in the micro-resistance term with a sharp Gaussian function.

The results of my numerical analysis indicated that when $J = 1.15$, $f = 0.03$, and $\epsilon = 0.85$ fractionalization could be observed within the simulation time. Furthermore, upon examining the magnetic profiles of numerical solutions for $\phi(x, t)$ we can see a bimodal distribution indicating a separation of fluxons. Once it was confirmed that separation took place, I calculated the tunneling rate Γ for both the large fluxon and the small fluxon. I found that while the smaller fluxon had a much smaller tunneling rate, the larger fluxon had a tunneling rate comparable to previous work done with single fluxons. It is reasonable that the smaller fluxon had much shorter

tunneling rate due to smaller relative mass compared to both the larger fluxon and a single fluxon. From the qualitative examination of the DSG, we can see that this is expected, as the smaller fluxon is $\approx 0.1644\Phi_0$, at $J = 1.15$. Future work to be done will be to investigate the phase dynamics with two micro-resistors acting as a double well potential in order to create a flux qubit.

BIBLIOGRAPHY

[1] "the schrödinger equation in a classical context". URL `https://www.feynmanlectures.caltech.edu/III_21.html`.

[2] An introduction to topological defects in field theories. URL `dbr@dartmouth.edu`.

[3] H Akoh, S Sakai, A Yagi, and H Hayakawa. Real time fluxon dynamics in josephson transmission line. *IEEE Transactions on Magnetics*, 21(2):737–740, 1985.

[4] Tuncay Aktosun, Francesco Demontis, and Cornelis Van der Mee. Exact solutions to the sine-gordon equation. *Journal of Mathematical Physics*, 51(12): 123521, 2010.

[5] John Argyris, Maria Haase, and Juan C Heinrich. Finite element approximation to two-dimensional sine-gordon solitons. *Computer methods in applied mechanics and engineering*, 86(1):1–26, 1991.

[6] O Astafiev, Yu A Pashkin, Yasunobu Nakamura, Tsuyoshi Yamamoto, and Jaw-Shen Tsai. Quantum noise in the josephson charge qubit. *Physical review letters*, 93(26):267007, 2004.

[7] DB Bailey, M Sigrist, and RB Laughlin. Fractional vortices on grain boundaries: the case for broken time-reversal symmetry in high-temperature superconductors. *Physical Review B*, 55(22):15239, 1997.

[8] A Barone, Floriana Lombardi, Giacomo Rotoli, and Francesco Tafuri. Macroscopic quantum phenomena in josephson structures. *Low Temperature Physics*, 36(10):876–883, 2010.

[9] Antonio Barone and Gianfranco Paterno. *Physics and applications of the Josephson effect.* Wiley, 1982.

[10] Karl K Berggren. Quantum computing with superconductors. *Proceedings of the IEEE*, 92(10):1630–1638, 2004.

[11] AJ Berkley, H Xu, MA Gubrud, RC Ramos, JR Anderson, CJ Lobb, and FC Wellstood. Decoherence in a josephson-junction qubit. *Physical Review B*, 68(6):060502, 2003.

[12] Curtis G. Callan and Sidney Coleman. Fate of the false vacuum. ii. first quantum corrections. *Phys. Rev. D*, 16:1762–1768, Sep 1977. doi: 10.1103/PhysRevD.16.1762. URL `https://link.aps.org/doi/10.1103/PhysRevD.16.1762`.

[13] David K Campbell, Michel Peyrard, and Pasquale Sodano. Kink-antikink interactions in the double sine-gordon equation. *Physica D: Nonlinear Phenomena*, 19(2):165–205, 1986.

[14] Jean-Guy Caputo and Denys Dutykh. Nonlinear waves in networks: a simple approach using the sine–gordon equation. *arXiv preprint arXiv:1402.6446*, 2014.

[15] Marcelo Cavalcanti, Nikolai Larkin, and J. Soriano. On solvability and stability of solutions of nonlinear degenerate hyperbolic equations with boundary damping. *Funkcialaj Ekvacioj. Serio Internacia*, 41, 01 1998.

[16] YM Cho and PM Zhang. Topological objects in two-gap superconductor. *The European Physical Journal B*, 65(2):155–178, 2008.

[17] John Clarke and Frank K Wilhelm. Superconducting quantum bits. *Nature*, 453 (7198):1031–1042, 2008.

[18] John Clarke, Andrew N Cleland, Michel H Devoret, Daniel Esteve, and John M Martinis. Quantum mechanics of a macroscopic variable: the phase difference of a josephson junction. *Science*, 239(4843):992–997, 1988.

[19] Shusa Deng, Lorenza Viola, and Gerardo Ortiz. Majorana modes in time-reversal invariant *s*-wave topological superconductors. *Phys. Rev. Lett.*, 108:036803, Jan 2012. doi: 10.1103/PhysRevLett.108.036803. URL `https://link.aps.org/doi/10.1103/PhysRevLett.108.036803`.

[20] Toshiaki Fujimori, Hideaki Iida, and Muneto Nitta. Field theoretical model of multilayered josephson junction and dynamics of josephson vortices. *Phys. Rev. B*, 94:104504, Sep 2016. doi: 10.1103/PhysRevB.94.104504. URL `https://link.aps.org/doi/10.1103/PhysRevB.94.104504`.

[21] T. A. Fulton, P. L. Gammel, D. J. Bishop, L. N. Dunkleberger, and G. J. Dolan. Observation of combined josephson and charging effects in small tunnel junction circuits. *Phys. Rev. Lett.*, 63:1307–1310, Sep 1989. doi: 10.1103/PhysRevLett.63.1307. URL `https://link.aps.org/doi/10.1103/PhysRevLett.63.1307`.

[22] Bal Ram Ghimire. Broken time reversal-symmetry state in a long josephson junction. *Journal of Institute of Science and Technology*, 20(2):115–121, 2015.

[23] Parag Ghosh, Jay D Sau, Sumanta Tewari, and S Das Sarma. Non-abelian topological order in noncentrosymmetric superconductors with broken time-reversal symmetry. *Physical Review B*, 82(18):184525, 2010.

[24] DR Gulevich and FV Kusmartsev. Flux cloning in josephson transmission lines. *Physical review letters*, 97(1):017004, 2006.

[25] Noriyuki Hatakenaka, Hideaki Takayanagi, Yoshihiro Kasai, and Satoshi Tanda. Double sine-gordon fluxons in isolated long josephson junctions. *Physica B: Condensed Matter*, 284:563–564, 2000.

[26] F. Hecht. New development in freefem++. *Journal of Numerical Mathematics*, 20(3-4):251 – 266, 01 Dec. 2012. doi: https://doi.org/10.1515/jnum-2012-0013. URL `https://www.degruyter.com/view/journals/jnma/20/3-4/article-p251.xml`.

[27] Zhao Huang and Xiao Hu. Josephson effects in three-band superconductors with broken time-reversal symmetry. *Applied Physics Letters*, 104(16):162602, 2014.

[28] Kenji Ishida, Yusuke Nakai, and Hideo Hosono. To what extent iron-pnictide new superconductors have been clarified: A progress report. *Journal of the Physical Society of Japan*, 78(6):062001, 2009. doi: 10.1143/JPSJ.78.062001. URL `https://doi.org/10.1143/JPSJ.78.062001`.

[29] BD Joesphson. Possible new effects in superconductive tunneling. *Phys. Lett*, 1 (7):251, 1962.

[30] Takeo Kato and Masatoshi Imada. Macroscopic quantum tunneling of a fluxon in a long josephson junction. *Journal of the Physical Society of Japan*, 65(9): 2963–2975, 1996.

[31] Ju H Kim. Quantum phase transitions in one-dimensional long josephson junction stacks in parallel magnetic fields. *Physical Review B*, 65(10):100509, 2002.

[32] Ju H Kim and Ramesh P Dhungana. Effects of a resonant cavity on macroscopic quantum tunneling of fluxons in long josephson junctions. *Physical Review B*, 83(6):064503, 2011.

[33] Ju H Kim and J Pokharel. Collective josephson vortex dynamics in long josephson junction stacks. *Physica C: Superconductivity*, 384(4):425–436, 2003.

[34] Ju H Kim, Ramesh P Dhungana, and Kee-Su Park. Decoherence in josephson vortex quantum bits: Long-josephson-junction approach to a two-state system. *Physical Review B*, 73(21):214506, 2006.

[35] Ju H Kim, Bal-Ram Ghimire, and Hao-Yu Tsai. Fluxon dynamics of a long josephson junction with two-gap superconductors. *Physical Review B*, 85(13):134511, 2012.

[36] Yuri S Kivshar and Boris A Malomed. Interaction of a fluxon with a local inhomogeneity in a long josephson junction. *Physics Letters A*, 129(8-9):443–448, 1988.

[37] Thaddeus D Ladd, Fedor Jelezko, Raymond Laflamme, Yasunobu Nakamura, Christopher Monroe, and Jeremy Lloyd O'Brien. Quantum computers. *Nature*, 464(7285):45–53, 2010.

[38] Yuriy Makhlin, Gerd Schön, and Alexander Shnirman. Quantum-state engineering with josephson-junction devices. *Reviews of Modern Physics*, 73(2):357–400, 2001. ISSN 0034-6861. doi: 10.1103/revmodphys.73.357.

[39] John M Martinis. Superconducting phase qubits. *Quantum information processing*, 8(2-3):81–103, 2009.

[40] John M Martinis, S Nam, J Aumentado, and C Urbina. Rabi oscillations in a large josephson-junction qubit. *Physical review letters*, 89(11):117901, 2002.

[41] John M Martinis, S Nam, J Aumentado, KM Lang, and C Urbina. Decoherence of a superconducting qubit due to bias noise. *Physical Review B*, 67(9):094510, 2003.

[42] David W McLaughlin and Alwyn C Scott. Perturbation analysis of fluxon dynamics. *Physical Review A*, 18(4):1652, 1978.

[43] Koji Nakajima, Hideshi Ichimura, and Yutaka Onodera. Dynamic vortex motion in long josephson junctions. *Journal of Applied Physics*, 49(9):4881–4885, 1978.

[44] Samira Nazifkar, Kurosh Javidan, and Mohsen Sarbishaei. Interaction of double sine-gordon solitons with external potentials: an analytical model. *Chinese Physics Letters*, 33(12):120502, 2016.

[45] Manfred Sigrist. Time-reversal symmetry breaking states in high-temperature superconductors. *Progress of theoretical physics*, 99(6):899–929, 1998.

[46] Eitan Tadmor. A review of numerical methods for nonlinear partial differential equations. *Bulletin of the American Mathematical Society*, 49(4):507–554, 2012.

[47] C. C. Tsuei and J. R. Kirtley. Pairing symmetry in cuprate superconductors. *Rev. Mod. Phys.*, 72:969–1016, Oct 2000. doi: 10.1103/RevModPhys.72.969. URL https://link.aps.org/doi/10.1103/RevModPhys.72.969.

[48] William G Unruh. Maintaining coherence in quantum computers. *Physical Review A*, 51(2):992, 1995.

[49] C. Q. Xu, B. Li, J. J. Feng, W. H. Jiao, Y. K. Li, S. W. Liu, Y. X. Zhou, R. Sankar, Nikolai D. Zhigadlo, H. B. Wang, Z. D. Han, B. Qian, W. Ye, W. Zhou, T. Shiroka, Pabitra K. Biswas, Xiaofeng Xu, and Z. X. Shi. Two-gap superconductivity and topological surface states in taossi. *Phys. Rev.*

B, 100:134503, Oct 2019. doi: 10.1103/PhysRevB.100.134503. URL `https://link.aps.org/doi/10.1103/PhysRevB.100.134503`.

This script is run using the FreeFEM++ software, which is open source and can be downloaded here:

APPENDIX A

FREEFEM++ SCRIPT

```
// Replaced the mesh with a mesh symmetric about 0

real r0=-10.0,r1=10.0;

real s0=0,s1=1;

int n=999,m=1;

mesh Th=square(n,m,[r0+(r1-r0)*x,s0+(s1-s0)*y]);

//fespace Vh(th,[P1,P1]);

//Vh [uu,vv], [w,s];

plot (Th, wait=1);


// The quadratic Lagrangian elements to solve the DSG

fespace Vh(Th,P2);


// The space for the output

fespace Wh(Th,P1);


// Time discretization parameters

real Tf = 200.0; // Final simulation time

int M = 1000;  // Number of steps

int Nwrite = 10; // write the results every Nw time steps

real dt = Tf/M; // time step

real dt2 = dt*dt; // dt^2


// inital conditions
```

```
real L = 0.251; // the length of the LJJ

real u0 = 0.0; //the kink's initial speed

real z = 1.00;

real x01 = 2.0;//the kink's initial position

real x02 = -3.5;

real xp= 0.0; // The position of the microresistance

real yp= 0.00 ; // The position of the microresistance

real sq = sqrt(1.0-u0*u0); // inverse of the Lorentz factor

real J = 1.10; // The Josephson Coefficient

//real a=sqrt((J-1)/(J+1));

//real b= sqrt((J*J-1)/(4*J));

real f=  0.005; // Bias Current

real ep= 0.85; // Micro-Resistance

real alpha = 0.005 ;


// initialized first two time steps
Vh phi0 = z*4.0*atan(exp((x-x01)/sq)) + (1.0-z)*4.0*atan(exp((x-x02)/sq));
 // kink shape at t=0
Vh phi1 = z*4.0*atan(exp((x-x01)/sq))+(1.0-z)*4.0*atan(exp((x-x02)/sq));
 // kink shape at t=dt
Vh delta= 1.0*(1.0/(2*sqrt(alpha)*sqrt(pi))^2)*exp((-(x-xp)^2-(y-yp)^2)/(4*alpha));
 // alpha = 0.005
//// We save the initial condition:


//// We save the initial condition:
Wh phiW; // projection variable belonging to the P1 space
```

```
{
phiW = phi0;
ofstream file("Solution_SGE_0.txt");
file << "2 1 1 " << phiW[].n << " 2\n";
for (int k=0; k < phiW[].n ; k++)
file << phiW[][k] << endl;



// Weak formulation
Vh phi, psi;
Vh phiml;
Vh dphi = dx(phi);


int op = 1;


problem DSG(phi,psi,init=op,solver=CG) =
int2d(Th)(phi*psi + 0.5*dt2*(dx(phi)*dx(psi) + dy(phi)*dy(psi)))
 + int2d(Th)(0.5*dt2*(dx(phi0)*dx(psi) + dy(phi0)*dy(psi)))
 + int2d(Th)(((phi0 - 2.0*phi1) + dt2*sin(phi1)
 + dt2*(0.5*J)*sin(2.0*phi1)- dt2*f - ep*delta*dt2*sin(phi1))*psi);


// solving the DSG
// The main loop in time:
for (int j=1; j<=M; j++)
{
DSG;
```

```
op = 1;


{

// save the current solution for the post-processing later:

phiW = phi;

ofstream file("Solution_SGE2" + j + ".txt");

file << "2 1 1 " << phiW[].n << " 2\n";

for (int k=0; k < phiW[].n ; k++)

file << phiW[][k] << endl;

}


phiml = phi0;
phi0 = phi1; phi1 = phi;


if (j % Nwrite == 0) // if the time to output the result has come:


plot(phi,fill=true,dim=3,cmm="Double Sine-Gordon with Bias current and Pinning",

ColorScheme=1);

}

}
```

POTENTIAL MINIMIZATION SCRIPT

```c
#include <stdio.h>

#include <math.h>


int main(){


double J=1.05,a,b,mg;

double q1,q2,q;

double U1,U2,U3,U4,U5,U6,U,f,ep;

int i,j;


FILE* output;

FILE* output1;

FILE* output2;

output = fopen("MQTPotential.txt", "w");

output1 = fopen("MQTPotential1.txt", "w");

output2 = fopen("MQTPotential2.txt", "w");


a=sqrt((J-1)/(J+1));

b=sqrt((J*J-1)/(4*J));

f=0.01;

ep=0.5;


for(i=0; i<=60; i++){
```

```
for(j=0; j<=60; j++){

q1=-3+i*0.1+0.005;

q2=-3+j*0.1+0.005;

q = q1-q2;

mg=8.0*tanh(b*q1)*tanh(b*q2);


U1 = -(2*3.14-4*atanh(a))*(f)*q2;

U2 = 2*ep*(1-1/(1+(a)*(a)*(1/tanh(q2))*(1/tanh(q2))));

U3 = -4*atanh(a)*(f)*q1;

U4 = 2*ep*(1-1/(1+(a)*(a)*(tanh(q1))*(tanh(q1))));

U5 =((a*a)/(2*b*b))*(mg/(1-a*a))*log(cosh(b*q)*cosh(b*q)+a*a*sinh(b*q)*sinh(b*q));

U6 = 0.5*0.252264396*(exp(-0.85*b*q*b*q)+1/cosh(1.27*b*q));

U= U1+U2+U3+U4+U5+U6;


fprintf(output, "%f\t%f\t%f\n", q1,q2,U);
}
}


for(i=0;i<200;i++){

q1=-10+i*0.1+0.005;


U1 = -(2*3.14-4*atanh(a))*(f)*q1;

U2 = 2*ep*(1-1/(1+(a)*(a)*(1/tanh(q1))*(1/tanh(q1))));

U3 = -4*atanh(a)*(f)*q1;

U4 = 2*ep*(1-1/(1+(a)*(a)*(tanh(q1))*(tanh(q1))));
```

```c
fprintf(output2, "%f\t%f\n", q1,U1+U2);

fprintf(output1, "%f\t%f\n", q1,U3+U4);


}


fclose(output);

fclose(output1);

fclose(output2);

}
```